

Soluble Human TLR2 Ectodomain Binds Diacylglycerol from Microbial Lipopeptides and Glycolipids

Maximiliano J. Jiménez-Dalmaroni^{1,2,7}, Catherine M. Radcliffe^{1,8}, David J. Harvey¹, Mark R. Wormald¹,
Petra Verdino², Gary D. Ainge^{3,4}, David S. Larsen³, Gavin F. Painter³, Richard Ulevitch⁵, Bruce
Beutler^{6,9}, Pauline M. Rudd^{1,10}, Raymond A. Dwek¹, Ian A. Wilson^{2*}

¹Glycobiology Institute, Department of Biochemistry, University of Oxford, UK

²Department of Integrative Structural and Computational Biology,
and the Skaggs Institute for Chemical Biology,
The Scripps Research Institute, USA

³Industrial Research Limited, Carbohydrate Chemistry,
P.O. Box 31-310, Lower Hutt, New Zealand

⁴University of Otago, Dunedin, New Zealand

⁵Department of Immunology and Microbial Sciences, The Scripps Research Institute, USA

⁶Department of Genetics, The Scripps Research Institute, USA

⁷Current address: Division of Developmental Biology,
Cincinnati Children's Hospital Research Foundation, USA

⁸Current address: Lonza Biologics plc, Slough, Berkshire, UK

⁹Current address: Center for Genetics of Host Defense, UT Southwestern Medical Center, USA.

¹⁰Current address: NIBRT, Conway Institute University College Dublin, Ireland

To whom correspondence should be addressed: Ian A. Wilson, Department of Integrative Structural and
Computational Biology, The Scripps Research Institute, 10550 N. Torrey Pines Road, La Jolla, CA
92037, USA. Tel.: +1 858 784 9706; Fax: +1 858 784 2980. E-mail: wilson@scripps.edu.

Keywords: diacylglycerol ligands; lipoarabinomannan; lipoteichoic acid; FSL-1; TLR2.

2 **Abstract**

3 Toll-like receptors (TLRs) are key innate immune receptors that recognize conserved features of
4 biological molecules that are found in microbes. In particular, TLR2 has been reported to be
5 activated by different kinds of microbial ligands. To advance our understanding of the interaction
6 of TLR2 with its ligands, the recombinant human TLR2 ectodomain (hTLR2ED) was expressed
7 using a baculovirus/ insect cell expression system, and its biochemical as well as ligand binding
8 properties were investigated. The hTLR2ED binds synthetic bacterial and mycoplasmal
9 lipopeptides, lipoteichoic acid (LTA) from *Staphylococcus aureus*, and synthetic
10 lipoarabinomannan precursors from *Mycobacterium* at extracellular physiological conditions, in
11 the absence of its co-receptors TLR1 and TLR6. We also determined that lipopeptides and
12 glycolipids cannot bind simultaneously to hTLR2ED and that the phosphatidyl inositol
13 mannoside 2 (Pim2) is the minimal lipoarabinomannan structure for binding to hTLR2ED.
14 Binding of hTLR2ED to Pim4, which contains a diacylglycerol group with one of its acyl chain
15 containing 19 carbon atoms, indicates that hTLR2ED can bind ligands with acyl chains longer
16 than 16 carbon atoms. In summary, our data indicate that diacylglycerol is the ligand moiety of
17 microbial glycolipids and lipoproteins that bind to hTLR2ED and that both types of ligands bind
18 to the same binding site of hTLR2ED. The design of novel inhibitors of TLR2, based on their
19 ability to bind to the TLR2 but not activate the TLR2 signaling pathway, may lead to the
20 development of novel treatments for septic shock caused by Gram- positive bacteria.

21 _____

22 Toll-like receptors (TLRs) have emerged as one of the most important group of pattern-
23 recognition receptors in innate immunity. TLRs are type I transmembrane receptors that are

24 important for the initiation of immune responses against microbes. Ten different human TLRs
25 are known, some of which are located in the plasma membrane (TLR1 TLR2, TLR4, TLR5,
26 TLR6), while others are sequestered in internal compartments, including endosomes (TLR3,
27 TLR7, TLR8 and TLR9) [1-2].

28 TLR2 has been reported to recognize a different kind of microbial ligands that include
29 synthetic triacyl-lipopeptides [3], surfactant protein A [4], meningococcal porin b [5],
30 mycoplasmal lipopeptides and mycobacterial lipoarabinomannan [6]. This promiscuity in the
31 recognition of ligands has been partially explained by the association of TLR2 with other TLRs,
32 such as TLR1 and TLR6 [7], but in other cases, the activation of TLR2 was the result of the
33 presence of contaminants in the preparation of ligands [8]. The class B scavenger receptors,
34 cluster of differentiation 36 (CD36) and cluster of differentiation 14 (CD14), also contribute to
35 the ligand recognition process by TLR2 [9-11]. The crystal structure of a chimera between the
36 human TLR2/ TLR1 ectodomain fused to LRR repeats of a variable lymphocyte receptor (VLR)
37 in complex with the triacyl-lipopeptide Pam₃CSK₄ revealed that a hydrophobic pocket composed
38 from the central leucine-rich repeats 9-12 (LRRs 9-12) of TLR2 is the binding site for
39 Pam₃CSK₄ [12]. The crystal structures of a mouse TLR2 ectodomain (mTLR2ED)/VLR hybrid
40 in complex with TLR6 and Pam₂CSK₄, as well as mTLR2ED/VLR in complex with PE-DTPA, a
41 synthetic derivative of phosphatidylethanolamine, and LTA from *Streptococcus pneumoniae*
42 (*S.pneumoniae*) also uncovered similar findings [13]. While these are extremely important steps
43 to determine the recognition of ligands by TLR2, our knowledge of TLR2 interactions with its
44 different ligands is far from complete[14].

45 In order to investigate the binding of human TLR2 with the synthetic diacyl-lipopeptide FSL-
46 1 (fibroblast stimulating lipopeptide-1) and LTA from *S. aureus* and lipoarabinomannan

47 precursors, hTLR2ED was expressed employing a baculovirus/ insect cell expression system.
48 The biochemical properties of hTLR2ED and the interaction with its ligands were investigated.

49

50 **EXPERIMENTAL PROCEDURES**

51 *Cell Culture and cell line*-Sf-9 (Invitrogen) and Hi-5 (Invitrogen) insect cells were employed for
52 baculovirus generation and protein expression, respectively. Both cell lines were cultured in
53 suspension cultures in serum-free HyQ media (Hyclone) at 25°C under shaking conditions.

54 *Generation of hTLR2ED Profold ER1 baculovirus*- hTLR2ED (residues 19 to 590, NCBI
55 accession number NP_003255) with a C-terminal His₆-tag was amplified by PCR using
56 pCDNA3.1 CMV TLR2 flag plasmid as template. The PCR product was cloned in TopoXL PCR
57 (Invitrogen), and subcloned into the *Bam*HI and *Not*I sites of the pAcGP67A transfer vector (BD
58 Pharmigen). A baculovirus, which we call hTLR2ED Profold ER1, was generated by
59 homologous recombination of hTLR2ED pAcGP67A with ProfoldER1 linearized baculovirus
60 vector (AB vector). After 5 rounds of viral amplification, a titer of 1x10⁸ viruses/ml was
61 achieved. Fluorescence from Green Fluorescent Protein (GFP) encoded in the ProfoldER1
62 linearized baculovirus vector was monitored using an Axioplan Zeiss fluorescent microscope.

63 *Purification of recombinant hTLR2ED protein*- Six liter cultures of 1 x 10⁶ Hi-5 cells/ml
64 were infected with hTLR2ED Profold ER1 at an MOI of 1. The infected cells were incubated at
65 27°C for 5 days under shaking conditions. The supernatant collected after centrifugation was
66 buffer exchanged into phosphate-buffered saline (PBS) and concentrated to 100 ml with a Pall
67 Filtron Centramate concentrator device (Millipore) using membranes with a 30,000 Da
68 molecular weight cut-off (Amersham). Next, 5 ml Ni (II) Nitrilotriacetic acid (Ni-NTA) beads
69 and 20 mM imidazole were added and incubated overnight at 4°C with agitation. Subsequently,

70 Ni-NTA beads were separated from the supernatant by filtration and washed 3 times with 20 mM
71 imidazole and 300 mM NaCl, pH 8. Bound proteins were eluted from the Ni-NTA beads with
72 100 mM imidazole and 300 mM NaCl. Anionic exchange chromatography using a Mono Q
73 column (Pharmacia) followed by size exclusion chromatography using a Superdex 200 10/30
74 column (Pharmacia) were employed to purify hTLR2ED to homogeneity.

75 *Identification of recombinant hTLR2ED by liquid chromatography-mass spectrometry (LC-*
76 *MS) and Western blot analysis-* hTLR2ED was concentrated to 5 mg/ml and its purity was
77 analyzed by sodium dodecyl sulphate (SDS) PAGE. The band between 50 and 75 kDa was
78 excised, reduced with dithiothreitol (DTT, 10 mM), and digested with trypsin overnight before
79 being analyzed by nano LC-MS/MS (The Scripps Research Institute Center for Mass
80 Spectrometry). Peptides were identified using MASCOT. Protein expression of hTLR2ED was
81 also confirmed by a Western blot probing for the presence of the C-terminal His-tag of the
82 hTLR2ED construct. After proteins were electroblotted from an SDS PAGE to a PVDF
83 membrane, the PVDF membrane was blocked for 1 hour at room temperature with 3% bovine
84 serum albumin (BSA), 0.5 % Tween 20. Subsequently, the membrane was incubated overnight
85 with a 1/1000 dilution of a mouse IgG anti-penta His-tag antibody (Qiagen), washed 3 times with
86 0.5 % Tween 20 in PBS, and incubated for 1 hour at room temperature with a 1/5000 dilution of
87 rabbit peroxidase-conjugated anti-mouse IgG antibody (Pierce). After three washes with 0.5%
88 Tween 20 in PBS, the Western blot was developed using the Super Signal West Pico ECL
89 substrate (Pierce).

90 *Presence of disulfide bonds in hTLR2ED-* Purified hTLR2ED was incubated for 10 minutes
91 in a reducing buffer containing β -mercaptoethanol or in a non-reducing protein gel loading
92 buffer. The samples were then run on a SDS PAGE to determine any difference in

93 electrophoretic mobility that would indicate the presence of disulfide bonds in hTLR2ED. The
94 presence of disulfide bonds was also observed in hTLR2ED deglycosylated with
95 endoglycosidases Endo H and PNGase F. 10 µg of purified hTLR2ED were digested with 50
96 units of PNGase F (New England Biolab) or Endo H (New England Biolab) in native conditions
97 overnight at 37°C. The samples were examined by SDS PAGE under reducing and non-reducing
98 conditions.

99 *Analysis of hTLR2ED glycosylation-* The hTLR2ED band was excised from an SDS PAGE
100 gel, cut into 1 mm cubes, and frozen overnight. The gel pieces were washed with acetonitrile to
101 remove any reagents and then dried in a vacuum centrifuge. The dried gel pieces were rehydrated
102 and incubated with PNGase F (Boehringer) for 16 hours at 37°C. The supernatant was collected.
103 Distilled water was added to the gels, which were sonicated for 30 minutes, and the supernatant
104 retained. This procedure was repeated twice with acetonitrile, followed by sbpd water, finishing
105 with acetonitrile to maximize the recovery of glycans. Samples were then treated with an AG 50
106 x 12 (Biorad, HemelHemsptead UK) anion exchange resin to eliminate sodium. The solution was
107 filtered through a filter syringe to eliminate the resin and then labeled with 2-aminobenzamide
108 (2AB) using the Ludger Tag 2-AB labeling kit (Ludger limited, Oxford, UK). Excess label was
109 removed by ascending chromatography on 3 mm Whatmann paper with acetonitrile as the
110 solvent and the glycans were eluted with sbpd water. Glycans were examined by normal-phase
111 high performance liquid chromatography (NP-HPLC) as previously reported [15] and by matrix-
112 assisted laser desorption/ionization time-of-flight (MALDI-TOF) mass spectrometry. The HPLC
113 system consisted of a 2690 Alliance separation module (Waters, Milford, MA) with a 4.6 x 250
114 mm TSK Amide-80 column (Anachem, Luton, UK) and was equipped with a fluorescence
115 detector set at 420 nm and was calibrated against a dextran standard. The retention time of each

116 glycan was converted into glucose units (GU) by comparison with the elution times of a dextran
117 ladder. The experimental GU values were then referred to Glycobase, a relational database
118 (<http://glycobase.ucd.ie/cgi-bin/public/glycobase.cgi>), which stores information of glycan
119 structure according to its GU values. Preliminary structure assignments were made for each
120 peak. Exoglycosidase array digestions further confirmed these assignments. The 2-AB labeled
121 glycans were digested with α -glucosidase II (EC 3.2.1.20) and jack bean α -mannosidase (EC
122 3.2.1.24) at 37°C for 18 hours. Digested samples were passed through a protein-binding filter
123 (Micropure-EZ centrifugal devices, Millipore Corporation) to remove the enzymes from the
124 glycans, which were washed thoroughly with sbpd water. Finally, the glycans were separated by
125 NP-HPLC to determine the changes in GU values as a result of the enzyme digestions.

126 *Matrix-assisted laser desorption/ionization time-of-flight (MALDI-TOF) mass spectrometry-*
127 Samples were cleaned with a Nafion membrane and MALDI-TOF mass spectra were recorded
128 with a Waters TofSpec 2E mass spectrometer (Waters MS-Technologies, Manchester UK) in
129 positive ion reflectron mode with delayed extraction. The acceleration voltage was 20.0 kV and
130 the pulse voltage was 3.0 kV. Samples in 0.3 μ L of water were mixed with 0.3 μ L of matrix (a
131 saturated solution of 2,5-dihydroxybenzoic acid in acetonitrile) on the MALDI target and
132 allowed to dry under ambient conditions. The dry sample was then recrystallized from ethanol.

133 *Electrospray ionization (ESI) mass spectrometry-* Negative ion ESI MS/MS spectra were
134 recorded with a Waters Q-TOF Ultima Global mass spectrometer. Samples (about 50
135 pmoles/ μ L), cleaned with a Nafion membrane as above, in 1:1 (v:v) methanol:water were
136 infused with a Proxeon (ProxeonBiosystems, Odense, Denmark (now part of Thermo Scientific))
137 borosilicate capillary. The ion source was maintained at 120°C, the infusion needle potential was
138 1.1 kV, the cone was at 100 V and the RF-1 voltage was 180 V. Spectra (2 sec scans) were

139 acquired with a digitization rate of 4 GHz. Collision-induced fragmentation (CID) data
140 acquisition used a 4 m/z mass window for parent ion selection and argon at approx 0.5 mBar as
141 the collision gas. The collision cell voltage was 80-120 V, depending on the parent ion mass and
142 other voltages were as recommended by the manufacturer. The instrument was externally
143 calibrated with *N*-glycans released from bovine fetuin and monoisotopic masses are cited to one
144 decimal place. Instrument control, data acquisition and processing were performed with a
145 MassLynx data system (Version 4.0).

146 *Circular Dichroism (CD) analysis of purified hTLR2ED-* CD measurements of hTLR2ED
147 were performed in 50 mMNaCl, 10 mMTrisHCl buffer at a concentration of 3.5 μ M on an AVIV
148 202 spectropolarimeter equipped with a thermostat (Hellma, Mullheim, Baden, Germany). The
149 purified hTLR2ED solution was placed in a 1 mm path length quartz cuvette and heated from
150 25°C-95°C at a rate of 1°C/minute. Spectra were recorded every 5°C after equilibration of 5
151 minutes at the corresponding temperature. The scans were performed in duplicate from 260 to
152 200 nm with 0.5 nm resolution. The spectra from duplicate scans were averaged and base-line
153 corrected by subtracting the corresponding buffer spectrum obtained under identical conditions.
154 Results were expressed as a mean residue ellipticity (Θ) at a given wavelength.

155 *Native PAGE experiments-* The following synthetic lipopeptides were employed for native
156 PAGE experiments: Cys-Ser-Lys₄ (CSK₄), *N*-palmitoyl Cys-Ser-Lys₄ (PamCSK₄), *S*-(2,3-*bis*-
157 palmitoyloxypropyl)-Cys-Ser-Lys₄ (Pam₂CSK₄), Pam₂CSK₄ fluorescein, *N*-palmitoyl-*S*-(2,3-
158 *bis*palmitoyloxypropyl)-Cys-Ser-Lys₄ (Pam₃CSK₄), *N*-palmitoyl-*S*-(2,3-*bis*-
159 palmitoyloxypropyl)-Cys-Ser-Lys₄, and *S*-(2,3-*bis*-palmitoyloxypropyl)-Cys-Gly-Asp-Pro-Lys-
160 His-Pro-Lys-Ser-Phe-K-Aca-Aca-Fluorescein (FSL-1-fluorescein) activator. All of these
161 synthetic lipopeptides were obtained from EMC Microcollection (Tubingen, Germany).

162 Lipoteichoic acid (LTA) and the human TLR9 ligand CpG-ODN2006 were obtained from
163 Invivogen (San Diego, CA, USA). Synthetic phosphatidylinositolmannosides (Pim2 and Pim4)
164 were synthesized as described previously[16-17]. The gp120 from HIV-1 clade B was a gift from
165 Dr. Robert Pejchal in our laboratory. 1 μ g of each of the mentioned compounds was separately
166 incubated with 10 μ g of hTLR2ED overnight at 37°C, pH 7.4. In case of the simultaneous
167 incubation with LTA and Pam₂CSK₄-fluorescein, 1 μ g of each compound were mixed and
168 incubated with 10 μ g of hTLR2ED. For the lipid ligands, an excess of ligands was added with
169 respect to hTLR2ED (ratio ligand/hTLR2ED: 11.3 (CSK₄), 8 (PamCSK₄), 5.41 (Pam₂CSK₄),
170 4.55 (Pam₃CSK₄), 6.53 (FSL-1), 3.7 (Pim2), 4.55 (Pim4), 2.9 (LTA)) because the lipid alone
171 forms aggregates due to hydrophobic interactions and, thus, it is difficult to calculate an accurate
172 ratio of monomeric ligand to hTLR2ED. The molar ratio of hTLR2ED to gp120 was 1.7:1. All
173 samples were run for 3 hours at 100 volts in a 4-20% native PAGE. Fluorescence was
174 determined with a Versadoc imaging system equipped with an emission filter with a 60 nm
175 bandwidth (from 500 nm to 560 nm). Subsequently, the gel was stained with Coomassie Blue
176 and destained with a solution containing 20% methanol, 10% acetic acid and 1% glycerol. Gel
177 images were taken with a Versadoc gel imaging system.

178 *Modeling of hTLR2ED-FSL-1, hTLR2ED-LTA, hTLR2ED-LTA C19 hTLR2ED-Pim-2 and*
179 *hTLR2ED-Pim-4 complexes-* Molecular modeling was performed on a Silicon Graphics Indigo 2
180 workstation using Insight II and Discover software (Accelrys). Figures were produced using the
181 program Molscript [18]. The models of hTLR2ED in complex with various ligands were based
182 on the crystal structures of the hTLR2ED/VLR hybrid in complex with Pam₃CSK₄ (Protein Data
183 Bank (PDB) 2Z7X) [12]and the Nogo receptor (PDB 1OZN)[19]. Residues 27-508 were taken
184 from 2Z7X, while residues 509-585 are based on residues 236-309 of 1OZN. The model was

185 created by overlaying the backbone atoms of residues 500-509 of 2Z7X with residues 227-236 of
186 1OZN. Five disulfide bonds were added to the model, one in the N-terminal cap, two in the LRR
187 domain (LRR12-13 and LRR15-16) as present in 2Z7X and two C-terminal disulfide bonds,
188 which are conserved in Nogo receptor and hTLR2ED (Figure 1). High-mannose glycans were
189 attached to each of the four glycosylation sites (Asn-114, Asn-199, Asn-414, and Asn-442)
190 (Figure 1) .All four potential glycosylation sites were solvent accessible. N-glycan structures
191 were generated using the database of glycosidic linkage conformations [20] and *in vacuo* energy
192 minimization to relieve unfavorable steric interactions. The Asn-GlcNAc linkage conformations
193 were based on the observed range of crystallographic values[20], the torsion angles around the
194 Asn C α -C β and C β -C γ bonds then being adjusted to eliminate unfavorable steric interactions
195 between the glycans and the protein surface. The complexes involving ligands with C16 acyl
196 chains were modeled simply by replacing the ligand head group of the crystallographic
197 Pam₃CSK₄ as appropriate. All of the modeled head groups could be accommodated with no need
198 to adjust any of the rest of the structure. The complexes of hTLR2ED with a C19 ligand (LTA
199 C19) and Pim4 were modeled by keeping the head group position constant and allowing the
200 protein structure to alter to accommodate the increased acyl chain length. This process was
201 carried out by increasing the chain length one carbon at a time and using molecular dynamic
202 simulations to allow relaxation of the local protein structure, while keeping the ligand head
203 group and the regions of the protein that do not interact with the acyl chains fixed. This resulted
204 in three of the outer-face loops changing their conformation slightly.

205 **RESULTS**

206 *hTLR2ED is expressed a monomer in insect cells with internal disulfide bonds and high-*
207 *mannose sugars-* The hTLR2ED, consisting of an N-terminal cap, an LRR domain, a C-terminal

208 cap, and a C-terminal His-tag, was successfully expressed using a baculovirus/ insect cell
209 expression system. Baculovirus for expression of hTLR2ED was generated by homologous
210 recombination of a plasmid encoding hTLR2ED and linearized baculovirus DNA. Baculovirus
211 amplification was monitored by fluorescent microscopy to detect expression of GFP encoded by
212 the baculovirus DNA. After three steps of purification, highly purified hTLR2ED was obtained
213 (Figure 2A). Moreover, hTLR2ED ran as an apparent monomer on size exclusion
214 chromatography by comparison with molecular weight standards (Figure 2B). Digestion of
215 hTLR2ED with PNGase F under native condition indicated the presence of N-linked
216 glycosylation (Figure 2C). The decreased electrophoretic mobility of native and deglycosylated
217 hTLR2ED under reducing conditions in the presence of β -mercaptoethanol was indicative of the
218 presence of disulfide bonds (Figures 2D, E). This finding is consistent with the reported crystal
219 structure of hTLR2ED which reveals disulfide bonds in the N-terminal cap and in the LRR
220 domain [10]. The identity of hTLR2ED was confirmed by anti-His-tag Western blot and by LC-
221 MS peptide fingerprinting (Figures 3A-B). The theoretical molecular weight of the hTLR2ED
222 protein is 65,734 Da (ProtParam, SwissProt), while the molecular weight of the hTLR2ED
223 determined by MALDI TOF MS is 69,903 Da (Figure 3C). Digestion of hTLR2ED with
224 PNGase F under native condition indicated that this difference in mass is due to the presence of
225 N-linked glycosylation (Figure 2C). The hTLR2ED has four N-linked glycosylation sites, which
226 are necessary for its secretion[21], highlighting the importance of N-linked glycosylation in
227 correct folding and stability[22-24]. Furthermore, we determined the type of glycosylation by
228 releasing the N-linked glycans from recombinant hTLR2ED using in-gel digestion with PNGase
229 F. We labeled the glycans with a fluorescent tag, digested with glucosidase II and α -jack bean
230 mannosidase and analyzed their composition by HPLC with fluorescence detection (Figure 4A).

231 The N-linked glycans were also identified by MALDI-TOF (Figure 4B) and negative ion CID
232 mass spectrometry. These data indicate that hTLR2ED glycosylation is predominantly of the
233 high-mannose type, which is consistent with the absence of secondary glycan processing in
234 insect cells[25-26]. This result was further confirmed by glucosidase II and α -jack bean
235 mannosidase digestions. Thus, the main glycan structures found in hTLR2ED were
236 Fuc₁Man₃GlcNAc₂, Man₃GlcNAc₂, Man₉GlcNAc₂ and Man₉Glc₁GlcNAc₂ (Table 1).

237 *Thermal denaturation of hTLR2ED is an irreversible two-stage process-* The
238 CD spectrum of hTLR2ED at 25°C revealed a minimum between 215 and 220 nm (Figure 5A),
239 which is indicative of a protein fold dominated by β -sheet secondary structure [27]. Furthermore,
240 thermal denaturation of hTLR2ED, as monitored by CD spectroscopy, uncovered a two stage
241 process (Figures 5A, B). The first stage occurred between 45°C and 55°C and another transition
242 occurs between 90°C and 95°C (Figure 5A, B). After denaturation at 95°C, hTLR2ED was
243 slowly cooled back down to 25°C and another CD spectrum was recorded. This spectrum
244 showed no difference from the spectrum recorded at 95°C demonstrating that thermal
245 denaturation of hTLR2ED appears to be an irreversible process (Figure 5C).

246 *hTLR2ED does not bind gp120 from HIV-1-* The hTLR2ED was employed for binding to
247 gp120 from HIV-1, different lipopeptides, and glycolipids (Figure 6). Because levels of
248 soluble TLR2 have been shown to correlate with HIV progression and increase after anti-
249 retroviral treatment[28], we tested whether hTLR2ED ectodomain is able to recognize the
250 surface viral glycoprotein gp120 from HIV-1. We determined that hTLR2ED does not bind
251 gp120 as no complex was observed in native PAGE (Figure 7A).

252 *hTLR2ED binds synthetic diacylglycerol lipopeptides but not monoacylated lipopeptides-*
253 Native polyacrylamide gel electrophoresis (native PAGE) experiments showed that hTLR2ED

254 binds synthetic lipopeptides (Figures 7B, C). A gel shift in the presence of Pam₂CSK₄ and
255 Pam₂CSK₄-fluorescein (Pam₂CSK₄f), but not CSK₄ and Pam₁CSK₄, indicated that hTLR2ED
256 binds the two fatty acid chains linked to cysteinyl *S*-glycerol (Figures 7B, C) in accord with the
257 crystal structure of hTLR2ED-Pam₃CSK₄[12]. Likewise, the gel shift of hTLR2ED incubated
258 with Fibroblast Stimulating Factor-1 fluorescein (FSL-1f) also reflects recognition of the
259 palmitic acid chains connected to the cysteinyl *S*-glycerol of FSL-1 (Figure 7B). Binding of FSL-
260 1f to hTLR2ED was confirmed by co-localization of hTLR2ED with the fluorescence as with
261 Pam₂CSK₄f (Figure 6C). As expected, hTLR2ED does not bind synthetic human TLR9 ligand
262 CpG-ODN2006 [29-31] or the synthetic lipopeptide Pam₃CSK₄ (Figure 7B).

263 *hTLR2ED binds LTA from S. aureus but cannot bind Pam₂CSK₄ and LTA simultaneously-* A
264 considerable increase in the electrophoretic mobility was observed for the hTLR2ED-LTA
265 complex (Figure 8A), consistent with the presence of the polyglycerophosphate moiety in LTA
266 Interestingly, native PAGE of hTLR2ED co-incubated with both LTA from *S. aureus* and
267 synthetic Pam₂CSK₄f showed that hTLR2ED preferentially binds to LTA rather than to
268 Pam₂CSK₄f (Figures 8A, 8B).

269 *hTLR2ED binds synthetic phosphatidylinositol mannosides (Pim2 and Pim4)-* We also
270 determined whether hTLR2ED binds other important glycolipids, such as mycobacterial
271 phosphatidylinositol mannosides, which were previously shown to be ligands for the
272 TLR2/TLR1 heterocomplex [32]. For these binding assays, we employed synthetic phosphatidyl
273 inositol mannosides, which we previously showed to bind CD36, but did not induce TNF- α
274 secretion by macrophages [11]. We also found that hTLR2ED binds to lipoarabinomannan
275 precursors (Pim2 and Pim4) (Figure 8C). The negative charge of Pim2 increased the mobility in
276 the native gel of the complex hTLR2ED-Pim2. In contrast, the extra two mannose and the extra

277 three carbons in one of the acyl chains of Pim4 (Figure 6) increased the mobility of hTLR2ED-
278 Pim4 (Figure 8C). Previous published results showed that human TLR2 has an impaired
279 recognition of lipopeptides with acyl chains shorter than 16 carbons atoms (C16) [33] and can
280 recognize longer acyl chains than C16 [34]. We report here that human TLR2 can bind
281 glycolipids with an acyl chain of 19 carbons atoms(C19) demonstrating that human TLR2 can
282 indeed accommodate acyl chains longer than C16 in its hydrophobic binding pocket.Taken
283 together, these binding assays demonstrate that the presence of two acyl chains linked to glycerol
284 is the essential ligand moiety recognized by TLR2 ligands, and that both glycolipids and
285 lipopeptides bind to the same binding site in hTLR2ED. Based on the crystal structure of
286 hTLR2ED-Pam₃CSK₄ [12], we modeled the hTLR2ED- FSL-1, hTLR2ED-LTA, hTLR2-LTA
287 (C19), hTLR2ED-Pim2, hTLR2-Pim4 complexes (Figure 9, 10). No clashes were found between
288 any of the ligand head groups and hTLR2ED, indicating that the binding pocket of hTLR2ED
289 might accommodate all of these ligands without major structural rearrangements. In addition, our
290 models suggest that the hTLR2ED could also accommodate ligands with longer acyl chains than
291 C16 without displacement of the ligand head group and only slight conformational adjustments
292 of some of the loops on the outer face of hTLR2ED.

293 **DISCUSSION**

294 TLRs are one of the most important groups of receptors responsible for the recognition of
295 bacteria, virus, parasites and initiation of a host immune response. TLRs are pathogen pattern-
296 recognition receptors (PPRs) because they recognize conserved structures in macromolecules in
297 these microorganismsThe crystal structures of hTLR2ED-Pam₃CSK₄, mTLR2ED-Pam₂CSK₄,
298 and mTLR2ED-Pam₃CSK₄ showed that the two acyl chains connected to the cysteinyl *S*-glycerol
299 occupy the hydrophobic binding pocket of TLR2ED [12].

300 Our aim was to investigate binding of other relevant lipopeptides and glycopeptides to
301 hTLR2ED. To address this issue, we expressed and purified the complete ectodomain of human
302 TLR2 (hTLR2ED) using a baculovirus expression system. The purified hTLR2ED is a monomer
303 in solution with intramolecular disulfide bonds and N-linked glycosylation of the high-mannose
304 type. It is likely that, besides disulfide bonds in the N-terminal cap and LRR domain, two
305 disulfide bonds are also likely to be present in the C-terminal cap domain (Figure 1). This
306 assumption is based on the observation of disulfide bonds in similar positions in hTLR3ED [35-
307 37] and the Nogo receptor [19]. Employing CD spectroscopy we followed the thermal stability
308 of hTLR2ED. We employed different algorithms to determine the remaining secondary structure,
309 but did not obtain a satisfactory result, as the theoretical curves were statistically far away from
310 the experimental curves. Although some secondary structure remains at 50°C, the majority of the
311 secondary structure appears to be lost at 95°C as the curve shifts to a peak of 208 nm (random
312 coil). Furthermore, although we did not measure the aggregation state, it is likely that the loss of
313 secondary structure shown as the curve shifts to 208 nm would expose to the solvent the
314 hydrophobic residues of the LRR motifs and result in aggregation. The relatively low value of
315 ~45-55°C for the first melting point of hTLR2ED suggests that its secondary structure is
316 thermally not very stable and might also indicate some structural flexibility. Asparagines
317 (“asparagine ladder”) and phenylalanines (“phenylalanine spine”) in the consensus LRR repeats
318 are known to be relevant for stabilization of LRR proteins through hydrogen bond formation and
319 hydrophobic interactions, respectively [38]. The lack of those particular features in the central
320 LRR repeats of hTLR2ED [12] (Figure 1) may render this domain more flexible and able to
321 accommodate ligands with long acyl chains, thereby contributing to an explanation of its low
322 melting point. We have tried other binding methods such as Surface Plasmon Resonance but did

323 not achieve satisfactory results. Thus, we decided to employ native PAGE which we have also
324 successfully employed to study the binding to TLRs and accessory molecules: TLR3 with
325 dsRNA [35], CD36 with LTA, Pims, FSL-1 [11], MD-1 with LPS [39], and TLR5 with flagellin
326 [40]. EMSA has also been successfully reported to study the binding between LTA-CD14 [41]
327 and TLR4-MD-2 with LPS [42]. Ligand binding alters the hydrodynamic size and/or charge of
328 the protein, which then manifests itself in different electrophoretic mobilities of the liganded and
329 unliganded forms. Here, we have demonstrated that hTLR2ED directly binds synthetic, diacyl-
330 (FSL-1 and Pam₂CSK₄) and triacyl-lipopeptides (Pam₃CSK₄), purified LTA from *S. aureus*, and
331 synthetic phosphatidylinositol mannosides (Pim2 and Pim4), in absence of TLR1 or TLR6.
332 Soluble isoforms of hTLR2ED present in plasma [43], breast milk [43,44], amniotic fluids [45],
333 saliva [46] and expressed in HEK cells [47] can act as a decoy of TLR2 and inhibit NFκB
334 activation by transmembrane TLR2 [48]. The hTLR2ED expressed in insect cells should have
335 the same inhibitory effect as the hTLR2ED from natural sources as the only difference with
336 them would be in the type of glycan structures, which should not be relevant for binding as the
337 glycosylation sites are not located near the binding site of hTLR2ED. Therefore, our ligand-
338 binding studies under physiological conditions suggest that ligand competition between secreted
339 isoforms of hTLR2ED and the transmembrane hTLR2 receptor is likely to be responsible for the
340 down-regulation of TLR2 activation. Soluble TLR2 has also been implicated in the pathogenesis
341 of HIV[28, 44]. Thus, we investigated whether hTLR2ED could interact with HIV-1 gp120. In
342 native PAGE experiments, we did not observe binding between hTLR2ED gp120 from HIV-1,
343 consistent with gp120 not being a lipoprotein.

344 One of the main classes of TLR2 ligands are microbial lipoproteins. Synthetic lipopeptides
345 can mimic the activity of microbial lipoproteins and, therefore, we investigated interaction of

346 these peptides with hTLR2ED. CSK₄ represents the amino-acid moiety of synthetic lipopeptides,
347 such as Pam₁CSK₄, Pam₂CSK₄, and Pam₃CSK₄. No appreciable differences were observed in the
348 electrophoretic mobility of hTLR2ED with and without CSK₄, demonstrating that hTLR2ED
349 does not interact with the amino-acid moiety of lipopeptides. Although no shift was seen for the
350 hTLR2ED-Pam₁CSK₄ complex, a complete gel shift is only observed when hTLR2ED binds
351 Pam₂CSK₄. Although we did not detect binding of Pam₁CSK₄ to hTLR2ED, it is still possible
352 that hTLR2ED may bind Pam₁CSK₄ with low affinity. The absence of the diacylglycerol moiety
353 in Pam₁CSK₄ explains its low biological activity compared to Pam₂CSK₄ [49].

354 The crystal structure of the hTLR2ED/hTLR1ED complex reveals that TLR2 binds the two acyl
355 chains linked to the cysteinyl S-glycerol of Pam₃CSK₄, and not the N-acyl chain which is bound
356 by TLR1. The two cysteinyl S-glycerol fatty acid chains can establish a greater number of
357 hydrophobic interactions and, thus, form a more stable complex with hTLR2ED.

358 Fibroblast-stimulating lipopeptide-1 (FSL-1) is a synthetic diacyl-lipopeptide that mimics the
359 N-terminal sequence of the 44-kDa lipoproteinLP44 of *Mycoplasma salivarium* [50-52]. FSL-1
360 is a potent activator of antigen-presenting cells and makes it a useful tool for treatment of cancer
361 and viral infections [53]. In native PAGE experiments, we observed that hTLR2ED binds
362 Pam₂CSK₄ and FSL-1 fluorescent ligands. FSL-1 shares the cysteinyl S-glycerolipid of
363 Pam₂CSK₄, but differs in the amino acids that are bound to the cysteine. Therefore, as in the case
364 of Pam₂CSK₄, hTLR2ED is likely to interact with the cysteinyl S-diacyl glycerol moiety of FSL-
365 1.

366 Peptidoglycan was thought to be a ligand for TLR2, but a recent report clearly showed that a
367 purified peptidoglycan shows no activity, and that earlier reported activity was caused by the
368 presence of contaminants, such as LTA[54]. Recent reports [55-58] also challenge the concept of

369 LTA as a ligand for TLR2, suggesting that its reported activity is actually caused by
370 contaminating lipoproteins. On the other hand, synthetic *S. aureus* LTA was reported to induce
371 secretion of TNF- α from whole blood cells and macrophages in a TLR2-dependent manner [59-
372 60].

373 Although peptidoglycan does not have fatty acid chains, LTA has a diacylglycerol structure
374 similar to FSL-1, Pam₂CSK₄, and Pam₃CSK₄. Here, we show a considerable increase in the
375 electrophoretic mobility of hTLR2ED after incubation with LTA from *S. aureus*. LTA from *S.*
376 *aureus* consists of up to 50 negatively charged glycerophosphate units linked to a gentiobiosyl
377 diacylglycerolipid that anchors the LTA to the plasma membrane [59], thus explaining the
378 increased electrophoretic mobility of the hTLR2ED-LTA complex compared to uncomplexed
379 hTLR2ED. Similarly increased electrophoretic mobility was shown for CD14-LTA and LBP-
380 LTA complexes as compared with unliganded proteins in native PAGE experiments [41]. We
381 also found that LTA can form aggregates with synthetic Pam₂CSK_{4f}, but that these complexes
382 are not recognized by hTLR2ED. In fact, the electrophoretic mobility of hTLR2ED incubated
383 with LTA and Pam₂CSK_{4f}, is identical to that obtained when hTLR2ED is incubated with LTA
384 alone. The acyl chains of the diacylglycerol anchor, as in the case of synthetic lipopeptides, are
385 likely to be the motif responsible for interaction with hTLR2ED. The crystal structure of
386 mTLR2ED/VLR in complex with LTA from *S. pneumoniae* also demonstrates the relevance of
387 the diacylglycerol of LTA as the ligand binding moiety recognized by TLR2[13]. However LTA
388 from *S. pneumoniae* has been shown to have an activity independent of TLR2 [58], showing that
389 binding to the hydrophobic pocket of TLR2 is necessary but not sufficient for a microbial ligand
390 to activate TLR2.

391 The acyl chains of LTA from *S. aureus* have a length between C14-C19 [59], while those in
392 Pam₂CSK₄ have only 16 carbon atoms (palmitates). Our modeling based on the published crystal
393 structure of TLR2 [12] shows that the hydrophobic pocket can accommodate longer fatty acid
394 chains than palmitic acid with minimal conformational changes to the outer loops of hTLR2ED.
395 Thus, the extra carbon residues of some LTA molecules could establish additional hydrophobic
396 interactions than Pam₂CSK₄ and could explain the preferential binding of hTLR2ED for LTA
397 from *S. aureus*. Therefore, the binding of Pim4, which has one of the two acyl chains composed
398 of 19 carbon atoms, confirm that TLR2 can accommodate ligands with acyl chains longer than
399 16 carbon atoms. Mycobacterium is an intracellular pathogen that lives inside macrophages,
400 inhibiting macrophage activation and phagosome maturation [61-63]. *Mycobacterium*
401 *tuberculosis* (*M. tuberculosis*) causes around two million deaths per year worldwide [64]. TLR2
402 has been shown to be important for controlling *M. tuberculosis* [65] and *Mycobacterium*
403 *leprae* (*M. leprae*) [66] infections. *Mycobacterium* possess a unique cell wall structure rich in
404 long fatty acids (mycolic acid), lipoglycans (lipoarabinomannan) and polysaccharides.
405 Lipoarabinomannan is composed of three structures: a phosphatidyl-mannosyl-*myo*-inositol
406 anchor (MPI), a polysaccharide backbone composed of D-arabinan and D-mannan, and
407 chemical structures attached to the arabinan core termed caps. According to the type of cap
408 motif, it is possible to classify lipoarabinomannans into three classes: if the cap is an
409 oligomannose type, it is termed ManLAM; if phosphatidylinositol, it is termed PILAM; and, if
410 no cap, it is termed AraLAM. PILAM is characteristic of fast growing mycobacteria, such as
411 *Mycobacterium. fortuitum* and *Mycobacterium smegmatis*, while slow growing mycobacteria,
412 such as *M. tuberculosis* and *M. leprae* ,have ManLAM structures in the cell wall. *Mycobacterium*
413 *chelonae* has araLAM in its cell wall [67]. Here, we show that the hTLR2ED is able to interact

414 directly with synthetic phosphatidylinositol mannosides, demonstrating that Pim2 is the minimal
415 lipoarabinomannan structure required for binding to the hTLR2ED. The phosphate group from
416 *myo*-inositol phosphate enables the hTLR2ED-Pim2 complex to run with increased
417 electrophoretic mobility compared to unliganded hTLR2ED. Changes in mobility of hTLR2ED-
418 Pim2 by oligomerization of hTLR2ED is unlikely as an oligomer should decrease the
419 electrophoretic mobility as for example TLR4 MD2 in complex with lipid A [42]. For Pim4, the
420 extra two mannose residues and extra three carbon residues in one of its fatty acid chains seem to
421 compensate for the negative charge of the phosphate group and make the complex hTLR2ED-
422 Pim4 run with decreased electrophoretic mobility than uncomplexed hTLR2ED. We have seen
423 similar decreased in mobility by addition of one acyl chain in the case of the complex of
424 hTLR2ED-Pam₃CSK₄ compared with hTLR2ED-Pam₂CSK₄. Although oligomerization of
425 hTLR2ED could be another explanation for the decreased in mobility of hTLR2ED in complex
426 with Pim4, Pam₃CSK₄ and Pam₂CSK₄, gel filtration of TLR2 ectodomain in complex with
427 lipopeptides and glycolipids has been reported before showing that there is no oligomerization of
428 TLR2 ectodomain [13].

429 It is likely that hTLR2ED also binds to the acyl chains linked to the diacylglycerol moieties, as
430 for lipopeptides.. Although synthetic Pim2 and Pim4 were able to bind TLR2, they were not able
431 to support TNF- α secretion from C57BL/6 [11]. Pims also have been shown to inhibit the
432 activation of TLR2 in a CD14 independent way [68], decrease allergic response [69, 70] and
433 affect dendritic cell maturation [71]. Lipoarabinomannan and phosphatidylinositol mannosides
434 were reported to be sensed by TLR1 and TLR2[41]. The failure to activate the TLR2 signalling
435 pathway by these synthetic Pims likely results from the lack of a third acyl chain, which is
436 necessary for TLR1 binding [72-73]. Therefore, the capacity of Pims to bind but not activate the

437 TLR2 signalling pathway could explain their inhibitory properties. The binding site of
438 hTLR2ED is situated in the convex while concave site of hTLR2ED is covered by
439 glycosylation, making it an unlikely site for binding ligands. The hydrophobic binding pocket of
440 hTLR2ED, situated in the transition between the central LRR domain and the C-terminal LRR
441 domain (LRR9-12), is the only binding site big enough to accommodate diacylglycerol structures
442 [12] what makes it unlikely that ligands binds to a secondary site even at the high concentration
443 of ligands employed. However, to discard any possible inespecific binding, future ligand
444 binding experiments employing hTLR2ED with mutation that abrogates ligand binding, such as
445 the mutation of Isoleucine 319 for Aspartate of the LRR 11 domain of human TLR2 [74]
446 (Figure 1), could be performed. Although we showed that *in vitro* conditions binding of
447 hTLR2ED with its ligands, where ligands concentration are higher than *in vivo* conditions. can
448 be performed in the abscense of accessory molecules such as CD36 or CD14, *in vivo* CD14 and
449 CD36 are relevant to efficiently load ligands into TLR2 and activate the TLR2-dependent
450 signalling [11]. Because of differences in the hydrophobic pocket of TLR2 between human and
451 other species, such as murine [33] and equine [76], mammals may not be suitable models for the
452 development of inhibitors for human TLR2. Instead, ligand binding assays such as those using
453 native PAGE may be a better approach for evaluating inhibitors for human TLR2.

454 In summary, we showed that hTLR2ED is able to bind synthetic FSL-1, Pim2, Pim4, and
455 LTA from *S. aureus* without the presence of its co-receptors TLR1 and TLR6. Although the
456 structures of ligands recognized by hTLR2ED are all different, they all share the presence of two
457 fatty acid chains linked to glycerol that is recognized by hTLR2ED (Figures 6, 9, 10). Overall,
458 our data indicate the presence of a single binding site in hTLR2ED for microbial glycolipids and
459 lipoproteins. Inhibitors with longer acyl chains than 16 carbon atoms, which bind but do not

460 activate TLR2 signaling, could represent a novel strategy for the treatment of septic shock
461 caused by Gram-positive bacteria.

References

1. Akira S. TLR signaling. *Curr Top Microbiol Immunol*. 2006;311:1-16.2. Moresco EM,
2. LaVine D and Beutler B. Toll-like receptors. *Curr Biol*. 2011;21:R488-493.
3. Vasselon T, Detmers PA, Charron D, et al. TLR2 recognizes a bacterial lipopeptide through direct binding. *J Immunol*. 2004;173:7401-7405.
4. Murakami S, Iwaki D, Mitsuzawa H, et al. Surfactant protein A inhibits peptidoglycan-induced tumor necrosis factor-alpha secretion in U937 cells and alveolar macrophages by direct interaction with toll-like receptor 2. *J Biol Chem*. 2002;277:6830-6837.
5. Massari P, Visintin A, Gunawardana J, et al. Meningococcal porin PorB binds to TLR2 and requires TLR1 for signaling. *J Immunol*. 2006;176:2373-2380.
6. Li J, Lee DS, Madrenas J. Evolving Bacterial Envelopes and Plasticity of TLR2-Dependent Responses: Basic Research and Translational Opportunities. *Front Immunol*. 2013; 4347.
7. Ozinsky A, Underhill DM, Fontenot JD, et al. The repertoire for pattern recognition of pathogens by the innate immune system is defined by cooperation between toll-like receptors. *Proc Natl Acad Sci U S A*. 2000;97:13766-13771.
8. Zähringer U, Lindner B, Inamura S, et al. TLR2-promiscuous or specific?. A critical re-evaluation of a receptor expressing apparent broad specificity. *Immunobiology*, 2008; 2013; 205-24
9. Hoebe K, Georgel P, Rutschmann S, et al. CD36 is a sensor of diacylglycerides. *Nature*. 2005;433:523-527.
10. van Bergenhenegouwen J, Plantinga TS, Joosten LA. TLR2 & Co: a critical analysis of the complex interactions between TLR2 and coreceptors. *J Leukoc Biol*. 2013 94:885-902.
11. Jimenez-Dalmaroni MJ, Xiao N, Corper AL, et al. Soluble CD36 ectodomain binds negatively charged diacylglycerol ligands and acts as a co-receptor for TLR2. *PLoS One*. 2009;4:e7411.
12. Jin MS, Kim SE, Heo JY, et al. Crystal structure of the TLR1-TLR2 heterodimer induced by binding of a tri-acylated lipopeptide. *Cell*. 2007;130:1071-1082.
13. Kang JY, Nan X, Jin MS, et al. Recognition of lipopeptide patterns by Toll-like receptor 2-Toll-like receptor 6 heterodimer. *Immunity*. 2009;31:873-884.
14. Monie TP, Moncrieffe MC and Gay NJ. Structure and regulation of cytoplasmic adapter proteins involved in innate immune signaling. *Immunol Rev*. 2009;227:161-175.
15. Radcliffe CM, Arnold JN, Suter DM, et al. Human follicular lymphoma cells contain oligomannose glycans in the antigen-binding site of the B-cell receptor. *J Biol Chem*. 2007;282:7405-7415.
16. Ainge GD PN, Denis M, Hayman CM et al.. Phosphatidylinositol mannosides: Synthesis and adjuvant properties of phosphatidylinositol di- and tetramannosides. *Bioorg Med Chem*. 2006;14:7615-7624.

17. Zajonc DM, Ainge GD, Painter GF, et al. Structural characterization of mycobacterial phosphatidylinositol mannoside binding to mouse CD1d. *J Immunol.* 2006;177:4577-4583.
18. Kraulis P. MOLSCRIPT: a program to produce both detailed and schematic plots of protein structures. *J Appl Cryst.* 1991;24:946-950.
19. He XL, Bazan JF, McDermott G, et al. Structure of the Nogo receptor ectodomain: a recognition module implicated in myelin inhibition. *Neuron.* 2003;38:177-185.
20. Petrescu AJ, Milac AL, Petrescu SM, et al. Statistical analysis of the protein environment of N-glycosylation sites: implications for occupancy, structure, and folding. *Glycobiology.* 2004;14:103-114.
21. Weber AN, Morse MA and Gay NJ. Four N-linked glycosylation sites in human toll-like receptor 2 cooperate to direct efficient biosynthesis and secretion. *J Biol Chem.* 2004;279:34589-34594.
22. Rudd PM, Elliott T, Cresswell P, et al. Glycosylation and the immune system. *Science.* 2001;291:2370-2376.
23. Parodi AJ. Protein glucosylation and its role in protein folding. *Annu Rev Biochem.* 2000;69:69-93.
24. Zapun A, Darby NJ, Tessier DC, et al. Enhanced catalysis of ribonuclease B folding by the interaction of calnexin or calreticulin with ERp57. *J Biol Chem.* 1998;273:6009-6012.
25. Marchal I, Jarvis DL, Cacan R, et al. Glycoproteins from insect cells: sialylated or not? *Biol Chem.* 2001;382:151-159.
26. Harrison RL and Jarvis DL. Protein N-glycosylation in the baculovirus-insect cell expression system and engineering of insect cells to produce "mammalianized" recombinant glycoproteins. *Adv Virus Res.* 2006;68:159-191.
27. Greenfield NJ. Methods to estimate the conformation of proteins and polypeptides from circular dichroism data. *Anal Biochem.* 1996;235:1-10.
28. Heggelund L, Flo T, Berg K, et al. Soluble toll-like receptor 2 in HIV infection: association with disease progression. *AIDS.* 2004;18:2437-2439.
29. Hemmi H, Takeuchi O, Kawai T, et al. A Toll-like receptor recognizes bacterial DNA. *Nature.* 2000;408:740-745.
30. Kerkmann M, Rothenfusser S, Hornung V, et al. Activation with CpG-A and CpG-B oligonucleotides reveals two distinct regulatory pathways of type I IFN synthesis in human plasmacytoid dendritic cells. *J Immunol.* 2003;170:4465-4474.
31. Zhang Y, Palmer GH, Abbott JR, et al. CpG ODN 2006 and IL-12 are comparable for priming Th1 lymphocyte and IgG responses in cattle immunized with a rickettsial outer membrane protein in alum. *Vaccine.* 2003;21:3307-3318.
32. Oliveira-Nascimento L, Massari P, Wetzler LM. The Role of TLR2 in Infection and Immunity. *Front Immunol.* 2012; 3: 79.
33. Grabiec A, Meng G, Fichte S, Bessler W, Wagner H, Kirschning CJ.(2004) Human but not murine toll-like receptor 2 discriminates between tri-palmitoylated and tri-lauroylated peptides. *J. Biol. Chem.* 2004; 279:48004-12
34. Buwitt-Beckmann U, Heine H, Wiesmüller KH, Jung G, Brock R, Ulmer AJ (2005) Lipopeptide structure determines TLR2 dependent cell activation level. *FEBS J.* 272: 6354-64
35. Choe J, Kelker MS and Wilson IA. Crystal structure of human toll-like receptor 3 (TLR3) ectodomain. *Science.* 2005;309:581-585.

36. Bell JK, Botos I, Hall PR, et al. The molecular structure of the Toll-like receptor 3 ligand-binding domain. *Proc Natl Acad Sci U S A*. 2005;102:10976-10980.
37. Bell JK, Askins J, Hall PR, et al. The dsRNA binding site of human Toll-like receptor 3. *Proc Natl Acad Sci U S A*. 2006;103:8792-8797.
38. Bell, J.K., Mullen GE, Leifer CA, et al., Leucine-rich repeats and pathogen recognition in Toll-like receptors. *Trends Immunol*, 2003; 24: 528-33.
39. Yoon, SI, Hong M, Hang GW, et al. Crystal structure of soluble MD-1 and its interaction with lipid IVA. *Proc Natl Acad Sci U S A*. 2010; 107: 10990-5
40. Yoon, SI, Kursanov O, Natajara V, et al. Structural basis of TLR5-flagellin recognition and signalling. *Science*. 2012; 335: 859-64
41. Song DH and Lee J-O, Sensing of microbial molecular patterns by Toll-like receptors. *Immunological Reviews*. 2012, 250:216-229
42. Kim HM, Park BS, Kim JI, et al. Crystal structure of the TLR4-MD-2 complex with bound endotoxin antagonist Eritoran. *Cell*. 2007;130:906-917.
43. LeBouder E, Rey-Nores JE, Rushmere NK, et al. Soluble forms of Toll-like receptor (TLR)2 capable of modulating TLR2 signaling are present in human plasma and breast milk. *J Immunol*. 2003;171:6680-6689.
44. Henrick BM, Nag K, Yao XD, et al. Milk matters : soluble Toll-like receptor 2 (sTLR2) in breast milk significantly inhibit HIV-1 infection and inflammation. *PLoS One*. 2012;7:e 40138.
45. Dulay AT, Buhimschi CS, Zhao G, et al. Soluble TLR2 is present in human amniotic fluid and modulates the intraamniotic inflammatory response to infection. *J Immunol*. 2009;182:7244-7253.
46. Kuroishi T, Tanaka Y, Sakai A, et al. Human parotid saliva contains soluble toll-like receptor (TLR) 2 and modulates TLR2-mediated interleukin-8 production by monocytic cells. *Mol Immunol*. 2007; 44: 1969-76
47. Raby AC, Le Bouder E, Colmont C, et al. Soluble TLR2 reduces inflammation without compromising bacterial clearance by disrupting TLR2 triggering. *J Immunol*. 2009;183:506-517.
48. Liew FY, Xu D, Brink E. et al. Negative regulation of toll-like receptor mediated immune response. *Nat Rev Immunol*. 2005; 5: 446-58
49. Meng G, Grabiec A, Vallon M, et al. Cellular recognition of tri-/di-palmitoylated peptides is independent from a domain encompassing the N-terminal seven leucine-rich repeat (LRR)/LRR-like motifs of TLR2. *J Biol Chem*. 2003;278:39822-39829.
50. Nakamura J, Shibata K, Hasebe A, et al. Signaling pathways induced by lipoproteins derived from *Mycoplasma salivarium* and a synthetic lipopeptide (FSL-1) in normal human gingival fibroblasts. *Microbiol Immunol*. 2002;46:151-158.
51. Okusawa T, Fujita M, Nakamura J, et al. Relationship between structures and biological activities of mycoplasmal diacylated lipopeptides and their recognition by toll-like receptors 2 and 6. *Infect Immun*. 2004;72:1657-1665.
52. Shamsul HM, Hasebe A, Iyori M, et al. The Toll-like receptor 2 (TLR2) ligand FSL-1 is internalized via the clathrin-dependent endocytic pathway triggered by CD14 and CD36 but not by TLR2. *Immunology*. 130:262-272.
53. Rose WA, 2 ND, McGowin CL, Pyles RB . FSL-1 a bacterial derived toll-like receptor2/6 agonist, enhances resistance to experimental HSV-2 infection. 2009; *Virol. J*. 6:195.
54. Travassos LH, Girardin SE, Philpott DJ, et al. Toll-like receptor 2-dependent bacterial sensing does not occur via peptidoglycan recognition. *EMBO Rep*. 2004;5:1000-1006.

55. Hashimoto M, Tawaratsumida K, Kariya H, et al. Not lipoteichoic acid but lipoproteins appear to be the dominant immunobiologically active compounds in *Staphylococcus aureus*. *J Immunol*. 2006;177:3162-3169.
56. Hashimoto M, Furuyashiki M, Kaseya R, et al. Evidence of immunostimulating lipoprotein existing in the natural lipoteichoic acid fraction. *Infect Immun*. 2007;75:1926-1932.
57. Fischer K, Stein K, Ulmer AJ, Lindner B, Heine H, Holst O. Cytokine-inducing lipoteichoic acids of the allergy-protective lactococcus lactis G121 do not activate via Toll-like receptor 2. *Glycobiology*. 2011 Dec;21(12):1588-95.
58. Gisch N, Kohler T, Ulmer AJ, Müthing J, Pribyl T, Fischer K, Lindner B, Hammerschmidt S, Zähringer U. Structural reevaluation of *Streptococcus pneumoniae* Lipoteichoic acid and new insights into its immunomodulatory potency. *J Biol Chem*. 2013 May 31; 288:15654-67.
59. Deininger S, Figueroa-Perez I, Sigel S, et al. Definition of the cytokine inducing minimal structure of lipoteichoic acid using synthetic derivatives. *Clin Vaccine Immunol*. 2007.
60. Morath S, Stadelmaier A, Geyer A, et al. Synthetic lipoteichoic acid from *Staphylococcus aureus* is a potent stimulus of cytokine release. *J Exp Med*. 2002;195:1635-1640.
61. Deretic V and Fratti RA. *Mycobacterium tuberculosis* phagosome. *Mol Microbiol*. 1999;31:1603-1609.
62. Miller BH, Fratti RA, Poschet JF, et al. Mycobacteria inhibit nitric oxide synthase recruitment to phagosomes during macrophage infection. *Infect Immun*. 2004;72:2872-2878.
63. Vergne I, Fratti RA, Hill PJ, et al. *Mycobacterium tuberculosis* phagosome maturation arrest: mycobacterial phosphatidylinositol analog phosphatidylinositol mannoside stimulates early endosomal fusion. *Mol Biol Cell*. 2004;15:751-760.
64. Briken V and Miller JL. Living on the edge: inhibition of host cell apoptosis by *Mycobacterium tuberculosis*. *Future Microbiol*. 2008;3:415-422.
65. Underhill DM, Ozinsky A, Smith KD, et al. Toll-like receptor-2 mediates mycobacteria-induced proinflammatory signaling in macrophages. *Proc Natl Acad Sci U S A*. 1999;96:14459-14463.
66. Krutzik SR, Ochoa MT, Sieling PA, et al. Activation and regulation of Toll-like receptors 2 and 1 in human leprosy. *Nat Med*. 2003;9:525-532.
67. Jankute M, Grover S, Rana AK, et al. Arabinogalactan and lipoarabinomannan biosynthesis: structure, biogenesis and their potential as drug targets. *Future Microbiol*. 2012; 7: 129-47.
68. Court N, Rose S, Bourigault ML, et al. Mycobacterial PIMs inhibit host inflammatory responses through CD14-dependent and CD14-independent mechanisms. *PLoS One*. 2011; 6 (9):e24631
69. Ainge GD, Hudson J, Larsen DS, Painter GF, et al. Phosphatidylinositol mannosides: synthesis and suppression of allergic airway disease. *Bioorg Med Chem*. 2006; 14: 5632-42
70. Harper JL, Hayman CM, Larsen DS, et al. A PIM₂ analogue suppresses allergic airway disease. *Bioorg Med Chem*. 2011; 19: 917-25
71. Mazurek J, Ignatowicz L, Kallenius G, et al. Divergent effects of mycobacterial cell wall glycolipids on maturation and function of human monocyte-derived dendritic cells. *PLoS One*. 2012; 7: e42515.
72. Gilleron M, Nigou J, Nicolle D, et al. The acylation state of mycobacterial lipomannans modulates innate immunity response through toll-like receptor 2. *Chem Biol*. 2006;13:39-47.
73. Gilleron M, Quesniaux VF and Puzo G. Acylation state of the phosphatidylinositol hexamannosides from *Mycobacterium bovis* bacillus Calmette Guerin and *mycobacterium*

tuberculosis H37Rv and its implication in Toll-like receptor response. *J Biol Chem.* 2003;278:29880-29889.

74 Kajava AV and Vasselon T. A network of hydrogen bond on the surface of TLR2 controls ligand positioning and cell signalling *J Biol Chem.* 2010; 285: 6227-6234

75. Irvine KL, Hopkins LJ, Gangloff M et al. The molecular basis for recognition of bacterial ligands at equine TLR2, TLR1 and TLR6. *Vet Res.* 2013; 44:50.

Acknowledgments- We thank Dr. Terry Butters for providing the α -glucosidase II as well as helpful discussions, Julie Vanhnasy for technical support, and Drs. Robyn Stanfield and Adam Corper for comments and suggestions for the manuscript. This study was supported by NIH grant AI42266 (IAW), and by a Joint Scripps/Oxford Graduate Scholarship. We also thank the Wellcome Trust for grants to purchase the ToFSpec and Q-TOF mass spectrometers and the Oxford Glycobiology Bequest for additional funding.

The abbreviations used are: TLRs:toll-like receptors; hTLR2ED: human toll-like receptor 2 ectodomain; HIV: human immunodeficiency virus; LTA: lipoteichoic acid; gp120: glycoprotein 120; Pim2: phosphatidyl inositol mannoside 2; GPI:glycosylphosphatidylinositol; C19: 19 carbon atoms; FSL-1: fibroblast stimulating lipopeptide-1; FSL-1f: fibroblast stimulating lipopeptide-1 fluorescein; EMSA:electrophoretic mobility shift assay; ESI:electrospray ionization; CD:cluster of differentiation; VLR:variable lymphocyte receptor (VLR); 2-AB: 2-aminobenzamide; ODN:oligodeoxynucleotide; Pam₃CSK₄:tripalmitoyl-cysteinyl-seryl-(lysyl)₃-lysine; Pam₂CSK₄:dipalmitoyl-cysteinyl-seryl-(lysyl)₃-lysine; Pam₂CSK₄f: dipalmitoyl-cysteinyl-seryl-(lysyl)₃-lysine fluorescein; PamCSK₄:palmitoyl-cysteinyl-seryl-(lysyl)₃-lysine; CSK₄: cysteinyl-seryl-(lysyl)₃-lysine GFP: green fluorescent protein; PBS: phosphate buffer saline; PPRs: pattern-recognition receptors; Man: mannose; Glc: glucose,Fuc; fucose; GlucNac: N-acetylglucosamine, A1: mono-antennary; Gal: galactose; Ni-NTA: nickel-nitriloacetic acid;

LRR:leucine-rich repeats; HPLC: high-performance liquid chromatography; FPLC: fast protein liquid chromatography; MS: mass spectrometry; MALDI TOF: matrix-assisted laser desorption and ionization time of flight, *S. aureus*: *Staphylococcus aureus*; *S. pneumoniae*: *Streptococcus pneumoniae*; *M*: *Mycobacterium*

Competing interest: The authors have declared that they have no competing interests.

Figure legends

Figure 1. Protein sequence of hTLR2ED employed for modelling with its ligands.

hTLR2ED has 20 predicted LRR repeats which are capped at its N-terminal (LRR-NT) and a C-terminal (LRR-CT). The individual LRRs of hTLR2ED were aligned based on the hTLR2ED/VLR crystal structure solved by Jin et.al[10]. The N-terminal, Central and C-terminal LRRs are indicated in red, blue and green, respectively. Cysteines that are shown to form disulfide bond in the crystal structure solved by Jin et.al[10] and cysteines from the C-terminal cap that are predicted to form disulfide bonds are color matched. Asparagines that are the potential glycosylation sites are highlighted in dark brown and the N-linked glycosylation consensus sequences are highlighted in yellow. The LRR consensus sequence are depicted and the position of the β strand is indicated by an arrow. The binding site in hTLR2ED is formed by LRR9, LRR 10, LRR 11 and LRR 12[10]. Mutation in the isoleucine 319 in the LRR11 (depicted in orange) has been reported [74] to abrogate the binding of TLR2 to Pam₃CSK₄

Figure 2. hTLR2ED expression and purification from insect cell culture. A) Culture supernatants of insect cells infected with hTLR2ED Profold ER1 were concentrated and purified

to homogeneity by Ni-NTA affinity, anion exchange and gel filtration chromatography. Samples were analyzed on 4–20% SDS-PAGE and stained with Coomassie Blue. **B)**hTLR2ED is a monomer in solution. Purified hTLR2ED and molecular weight standards were run on a Superdex 200 10/30 gel filtration column. Purified hTLR2 ED elutes at 14.2 ml, which corresponds to the elution volume of a protein of 70,000 Da, which is approximately the molecular mass of the hTLR2ED monomer(n.b. the molecular weight of the hTLR2ED monomer as determined by MALDI TOF mass spectrometry is 69,903 Da).**C)**hTLR2ED has N-linked glycosylation. hTLR2 undigested (1) and digested overnight with PNGase F in native conditions (2).**D-E)** hTLR2ED contains intramolecular disulfide bonds. **D)** Purified hTLR2ED was run under reducing (1R) and non-reducing (2NR) conditions in an SDS PAGE gel. The difference in electrophoretic mobility indicates the presence of disulfide bridges. **E)**hTLR2ED was digested overnight at 37°C with PNGase F and Endo H and then run in SDS PAGE under reducing (1R) and non-reducing (2NR) conditions (E). Molecular weight markers are shown on each gel in kDa.

Figure 3. hTLR2ED expression using a baculovirus/ insect cell expression system **A)** The identity of the recombinant hTLR2ED was confirmed by LC-MS/MS. 19 peptides which cover 49% of hTLR2ED protein sequence were identified using MASCOT and depicted in red. **B)** The identity of the hTLR2ED was also confirmed by Western blot against its C-terminal His tag. **C)** The molecular weight was determined by mass spectrometry (TSRI mass spectrometry core).

Figure 4. hTLR2ED expressed in insect cells is glycosylated with high mannose N-linked sugars. **A)** HPLC chromatogram showing the profile of hTLR2ED glycans. The glycans were labeled with 2-AB and digested for 18 hours at 37°C with α -glucosidase II (Gluc II) and jack bean α -mannosidase (JBM) and run on a normal phase HPLC .An alternative nomenclature for

naming the glycan structures was employed which does not mention the two core N-acetylglucosamine (GlcNAc₂) which are present in all the glycan structures (for example: Man₂ corresponds to Man₂GlcNAc₂). **B)** MALDI-TOF mass spectrum of N-linked glycans released from hTLR2ED by PNGaseF treatment. The spectrum has been processed by the MaxEnt 2 algorithm from MassLynx (Waters). Ions at *m/z* 1036, 1179, 1341, 1375 and 1712 are contaminants. Symbols and abbreviations used for the structures: Man: mannose (open circle), Glc: glucose (open square), Fuc: core fucose (diamond with central dot), N-acetylglucosamine (filled square), and A1: mono-antennary.

Figure 5. Circular Dichroism analysis of hTLR2ED. **A)** CD spectra of hTLR2ED recorded at various temperatures. The CD spectrum of hTLR2ED at 25°C reveals a minimum around 215 nm that is indicative of a folded protein with a significant portion of β-sheet secondary structure. At temperatures greater than 50°C, the β-sheet character of the hTLR2ED CD spectra is lost and the shape of the spectra indicates that the hTLR2ED is now mostly unfolded. **B)** Thermal denaturation of hTLR2ED is a two-stage process. The CD signal at 208 nm was plotted against the corresponding temperatures. hTLR2ED undergoes two unfolding transitions: at the first *T_m* of 45-55°C, and a second *T_m* of 90-95°C, the protein becomes mostly unfolded. **C)** The thermal denaturation of hTLR2ED is irreversible. After the CD spectra of hTLR2ED were recorded at 95°C, hTLR2ED was slowly cooled back down to 25°C and new CD spectra were recorded (TLR2 post dT). There were no differences between the spectra at 95°C and after re-cooling, indicating that no secondary structure is regained and that the thermal denaturation of hTLR2ED is irreversible.

Figure 6. The chemical structures of lipopeptides and glycolipids employed for binding studies with hTLR2ED. The diacylglycerol moieties that are involved in the interaction with hTLR2ED are highlighted by boxes.

Figure 7. hTLR2ED binds diacyl and triacyllipopeptides, but not HIV-1 gp120. Samples were incubated overnight at 37°C and run for 4 hours at 100 volts on a native 4-20% native PAGE. Native gels stained with Coomassie Blue. **A)** hTLR2ED incubated with a clade B HIV-1 gp120. Lane 1- 10 µg of hTLR2ED; lane 2- 10 µg hTLR2ED with 10 µg gp120; lane 3- 1 µg hTLR2ED with 1 µg gp120; lane 4- 10 µg gp120. **B-C)** hTLR2ED incubated with lipopeptides. Native gel stained with Coomassie Blue (**B**) and corresponding fluorescence determined using a Versadoc imaging system (**C**). Lane 1-10 µg hTLR2ED with 1 µg FSL-1 fluorescein (FSL-1f); Lane 2- 1 µg FSL-1f; Lane 3-10 µg hTLR2ED with 1 µg Pam₂CSK₄ fluorescein (Pam₂CSK₄f); Lane 4-1 µg Pam₂CSK₄f; Lane 5-10 µg hTLR2ED with 1 µg Pam₂CSK₄; Lane 6-1 µg of Pam₃CSK₄;); Lane 7- 10 µg hTLR2ED; Lane 8-10 µg hTLR2ED with 1 µg ODN2006 (human TLR9 activator); Lane 9- 1 µg ODN2006; Lane 10-1 µg Pam₂CSK₄; Lane 11- 10 µg of hTLR2ED with 1 µg Pam₃CSK₄; Lane 12-10 µg hTLR2ED with 1 µg Pam₁CSK₄; Lane 13-10 µg hTLR2ED with 1 µg CSK₄. Fluorescence of Pam₂CSK₄f-hTLR2ED and FSL1f-hTLR2ED is indicated by arrows.

Figure 8. hTLR2ED binds LTA from *S. aureus* and mycobacterial Pims. **A-B)** hTLR2ED incubated with LTA and/or Pam₂CSK₄f. **A)** Native gel stained with Coomassie Blue and **B)** fluorescence determined using a Versadoc imaging system. Lane 1-10 µg hTLR2ED with 1 µg LTA; Lane 2- 1 µg hTLR2ED with 1 µg of LTA; Lane 3-10 µg hTLR2ED; Lane 4- 10 µg hTLR2ED with 1 µg Pam₂CSK₄ fluorescein (Pam₂CSK₄f); Lane 5-10 µg hTLR2ED with 1 µg

Pam₂CSK₄f and 1 μg LTA; Lane 6- 1 μg LTA; Lane 7- 1 μg Pam₂CSK₄f plus 1 μg LTA; Lane 8- 1 μg Pam₂CSK₄f. C)hTLR2ED incubated with Pims. Native gel stained with Coomassie Blue. Lane 1-10 μg hTLR2ED with 1μg Pim4; Lane 2- 10 μg hTLR2ED; Lane 3-10 μg hTLR2ED with 1μg of Pim2; Lane 4-1μg Pim2; Lane 5-1μg Pim4. The chemical structures of Pim4 and Pim2 are shown in Figure 3, with the two extra mannoses and extra three carbon atoms of Pim4 highlighted in red.

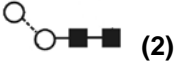
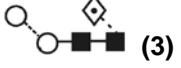
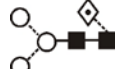
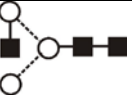
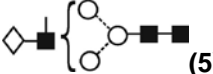
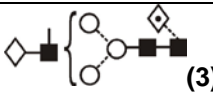
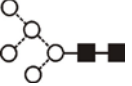
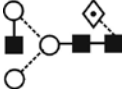
Figure 9. Modeling of hTLR2ED in complex with A) Pim2, B) Pim4, C) LTA, and D) LTA 19C, and E) FSL-1. Modeling is based on the crystal structures of hTLR2ED in complex with Pam₃CSK₄ (Protein Data Bank 2Z7X) [10] and the Nogo receptor (PDB 1OZN) [17] . The most abundant N-linked glycans from the glycan analysis were added to the hTLR2ED models: Man₃GlcNAc₂ (Asn114), Man₉GlcNAc₂ (Asn199), Man₃Fuc₁GlcNAc₂ (Asn414), Man₉Glc₁GlcNAc₂ (Asn442). All ligands have two acyl chains with 16 carbon atoms, except for LTA 19C, which has two acyl chains with 19 carbon atoms and Pim4 which has one acyl chain of 19 carbon atoms and another of 16 carbon atoms.

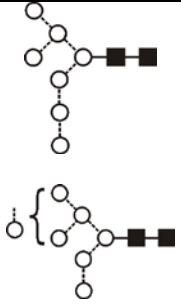
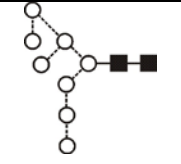
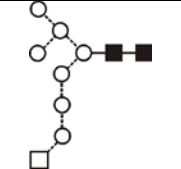
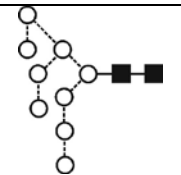
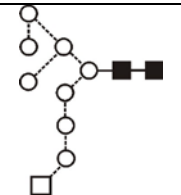
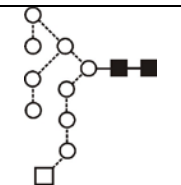
Figure 10. Zoom of the Figure 9 depicting the binding site of hTLR2ED in complex with A) Pim2, B) Pim4, C) LTA, and D) LTA 19C, and E) FSL-1.

Table 1. Percentages and Glucose unit values (GU) of the N-linked glycans of hTLR2ED expressed in insect cells. The most abundant glycan structures are Man₉Glc₁GlcNAc₂, Man₉GlcNAc₂, fucosylated-Man₃GlcNAc₂, Man₃GlcNAc₂. The alternative nomenclature of glycan structures, depicted in the HPLC Chromatogram, is shown in parentheses. References: GU glucose units: Man: mannose (open circle), Glc: glucose (open square), Gal: galactose

(diamond), Fuc:fuco (diamond with central dot), GlcNAc:*N*-acetylglucosamine (filled square), A1: mono-antennary. (1) Listed in order of GU value. (2) Not detected by mass spectrometry. (3) Not detected by ESI mass spectrometry; structure not confirmed by fragmentation. (4) Not detected by HPLC. (5) Trace amount by mass spectrometry; structure not confirmed by fragmentation. (6) As measured by HPLC.

Table1. Masses and structures of TLR2 glycans

Glycan assignment	GU(1)	m/z ([M+Na] ⁺)		m/z ([M+H ₂ PO ₄] ⁻)		Composition			Structure	% Total (6)
		Found	Calc.	Found	Calc.	Hex	HexNAc	Fuc		
Man ₂ GlcNAc ₂ (Man ₂)	3.40	-	771.3	-	845.2	2	2	0	 (2)	6.5
FucMan ₂ GlcNAc ₂ (FucMan ₂)	3.94	917.5	917.3	-	991.3	2	2	1	 (3)	10.3
Man ₃ GlcNAc ₂ (Man ₃)	4.37	933.5	933.3	1007.3	1007.3	3	2	0	 (2)	12.6
FucMan ₃ GlcNAc ₂ (FucMan ₃)	4.84	1079.6	1079.4	1153.4	1153.4	3	2	1	 (3)	17.5
GlcNAc Man ₃ GlcNAc ₂ (A ₁)	4.91	1136.5	1136.4	1210.4	1210.4	3	3	0	 (2)	5.7
GalGlcNAc Man ₃ GlcNAc ₂ (A ₁ G ₁)	(4)	-	1298.4	1372.4	1372.4	4	3	0	 (5)	(4)
FucGalGlcNAc Man ₃ GlcNAc ₂ (FucA ₁ G ₁)	(4)	-	1444.5	-	1518.5	4	3	1	 (3)	(4)
Man ₅ GlcNAc ₂ (Man ₅)	6.14	1257.5	1257.4	1331.4	1331.4	5	2	0	 (2)	2.9
FucGlcNAcMan ₃ GlcNAc ₂ (FucA ₁)	5.36	1282.6	1282.5	1356.5	1356.4	3	3	1	 (3)	3.1
Man ₆ GlcNAc ₂ (Man ₆)	7.06	1419.6	1419.5	1493.5	1493.5	6	2	0	 (Trace)	1.8

Man₇GlcNAc₂ (Man₇)	7.96	1581.6	1581.5	1655.5	1655.5	7	2	0		1.5
Man₈GlcNAc₂ (Man₈)	8.85	1743.5	1743.6	1817.6	1817.6	8	2	0		2.3
Glc₁Man₇GlcNAc₂ (Man₇Glc₁)	8.65									4.2
Man₉GlcNAc₂ (Man₉)	9.53	1905.5	1905.6	1979.6	1979.6	9	2	0		10.7
Glc₁Man₈GlcNAc₂ (Man₈Glc₁)	(4)									(4)
Glc₁Man₉GlcNAc₂ (Man₉Glc₁)	10.16	2067.7	2067.7	2141.7	2141.7	10	2	0		17.5
Unknown	9.73 10.36	-	-	-	-	-	-	-	-	3.4